Title

Level Crossing Resonance Studies of the Muoniated Cyclohexadienyl Radical (MuĊ6H6) Interacting with Uncapped Gold Nanoparticles in Porous Silica Hosts

Journal

The Journal of Physical Chemistry C, 125(39)

ISSN

1932-7447

Authors

Fleming, Donald G
MacFarlane, William A
Xiao, Jiyu
et al.

Publication Date

2021-10-07

DOI

10.1021/acs.jpcc.1c05723

THE JOURNAL OF PHYSICAL CHEMISTRY C
A JOURNAL OF THE AMERICAN CHEMICAL SOCIETY

pubs.acs.org/JPCC

Article

Level Crossing Resonance Studies of the Muoniated Cyclohexadienyl Radical ($Mu\dot{C}_6H_6$) Interacting with Uncapped Gold Nanoparticles in Porous Silica Hosts

Published as part of The Journal of Physical Chemistry virtual special issue "125 Years of The Journal of Physical Chemistry".

Donald G. Fleming,* William A. MacFarlane, Jiyu Xiao, Donald J. Arseneau, Robert F. Kiefl, Yuanyuan Cao, Peixi-X Wang, Mark J. MacLachlan, and Michael D. Bridges

Cite This: *J. Phys. Chem. C* 2021, 125, 21410−21423

Read Online

ACCESS | Metrics & More | Article Recommendations

ABSTRACT: The study of metal nanoparticles (NPs) and gold NPs (AuNPs), in particular, has been a subject of considerable interest in recent years. The present paper reports on the formation of the muoniated cyclohexadienyl radical in the Mu + C_6H_6 → $Mu\dot{C}_6H_6$ addition reaction in the same 8 and 10 nm AuNP samples, encapsulated in SBA-15 mesoporous silica, where the spin-relaxation rates λ_{Mu} were recently reported on [Fleming et al. *J. Phys. Chem. C*, **2019**, *123*, 27628, paper "P1"], but the final state was not identified in that study. The formation of this $Mu\dot{C}_6H_6$ radical and its interactions with the AuNP surfaces is investigated herein by the technique of avoided level crossing (ALC) resonance spectroscopy, for the same range of Bz loadings as studied earlier. The positions of the level crossings, giving the hyperfine coupling constants (hfcc) for the C−Mu and C−H bonds at the "ipso" position where Mu adds to the ring, are essentially the same as those seen in solid Bz and in bare silica, and hence these hfcc *do not* distinguish site locations for the surface-adsorbed benzene. The *amplitudes* of these resonances, which are a measure of the fraction of Mu forming the free-radical final state, do, however, provide such a distinction, being much less for Bz adsorbed in the AuNP/silica samples than in the bare silica. This loss in amplitude is attributed to competitive reaction channels, one forming the $Mu\dot{C}_6H_6$ free radical interacting with the AuNPs and the other due to formation of *diamagnetic* final states. An important signpost as to the nature of these competitive reaction channels is provided by the measured *widths* of the ALC resonances seen. These are surprisingly narrower in the presence of the AuNPs than for the bare silica, implying that the $Mu\dot{C}_6H_6$ radical is *not* in direct contact with the AuNPs. These differing possibilities and contrasting mechanisms are discussed.

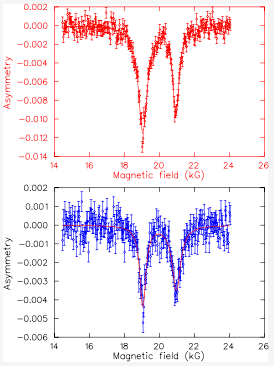

1. INTRODUCTION

Metal nanoparticles (NPs) and, here, gold NPs (AuNPs) are of general interest in the fields of surface science,[1] magnetism,[2−4] and catalysis,[5−10] with processes involving free radicals[5,11−18] in the latter regard being particularly relevant here. In order to explore the surface interactions of atoms and molecules with metal NP surfaces, it is essential that the NPs remain isolated and nonaggregating, which is often done by employing molecular capping agents, typically organic thiol groups.[1,2,4,19] However, these can change the nature and stability of metal NPs[20] and hence their surface reactivity. Recently, we explored hydrogen atom interactions with AuNPs utilizing the light hydrogenic H atom "muonium", composed of a positive muon and an electron (Mu = μ^+e^-, mass 0.114 amu[5,7,21−23]), in studies of its surface magnetism[3,4] and reactivity on AuNPs,[3,5,23] encapsulated in mesoporous (SBA-15) silica hosts.[3,11,23−25] The porous silica not only prevents the aggregation of the AuNPs but importantly also provides for measurements on *uncapped* NP surfaces.

Heterogeneous catalysis has been an important topic in the chemical sciences for many years,[9,26,27] in which oxide environments in general[28,29] and silicious environments in particular, including mesoporous silica[9,10,30,31] and zeolites,[32−34] have often been used as supports for catalytically active species. The acidic properties of such environments[32,34−36] are also important, via proton or H atom transfer reactions to guest molecules[7,12,27,32−34,37−39] that can also form free-radical intermediates, important to hydrogenation reactions in general[6,39] and for benzene in particular.[5,15,16,34,40] Other than from muon sci-

Received: June 29, 2021
Published: September 28, 2021

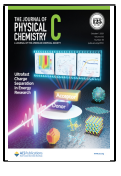

https://doi.org/10.1021/acs.jpcc.1c05723
J. Phys. Chem. C 2021, 125, 21410−21423

ence[11,13,22,41−46] though, exemplified by the present paper as well, there are very few examples of the *direct* observation of such H-adduct free radicals by spectroscopic techniques, notable exceptions relevant here being the $\dot{H}C_6H_6$ cyclohexadienyl radical seen in ZSM-5 zeolite[15] and the ethyl $CH_3\dot{C}H_2$ and $H\dot{C}_6H_6$ radicals interacting with PdNPs investigated by ESR in silica environments.[16] While ESR would generally be the technique of choice for the investigation of free radicals, the confined geometries of mesoporous silica[47] environments can facilitate radical−radical recombination reactions,[48] reducing signal amplitudes which are generally quite weak to begin with, particularly at higher temperatures, as well as likely affecting the measurements of reaction rates in such confined environments.[49]

The Mu atom has thus emerged as key in investigating the dynamics and hyperfine coupling constants of H-adduct free radicals in different environments, forming their muoniated isotopic equivalents[7,11,13,17,22,42−44] by Mu addition reactions, wherein the basic μSR (muon spin rotation, resonance, relaxation) technique effectively allows only *one* muoniated radical in the system at a time.[5,7,17,22,41,50,51] Though isotopic mass effects on measured hyperfine coupling constants are usually the principal theme of such studies, that is not the case here. Rather, the focus is on the direct observation of the muoniated cyclohexadienyl radical expected to form at AuNP sites in the

$$\begin{aligned} &\mathrm{Mu} + \mathrm{AuNP}/\mathrm{C_6H_6} \\ &\quad \xrightarrow{k_{\mathrm{Bz}}} \mathrm{Mu}\dot{\mathrm{C}}_6\mathrm{H}_6^{*}\cdot\mathrm{AuNP} \\ &\quad \xrightarrow{k_{\mathrm{S}}} \mathrm{Mu}\dot{\mathrm{C}}_6\mathrm{H}_6\cdot\mathrm{AuNP} \end{aligned} \qquad \text{(R1)}$$

addition reaction, proposed in ref 5 (hereafter referred to as paper "P1"), where k_{Bz} is a rate constant for the addition step and k_S is a rate constant for the stabilization of the $Mu\dot{C}_6H_6^*$ intermediate excited state (largely due to the exoergicity of the bond formed) on the AuNP surface, assumed to occur on a time scale much faster than its dissociation back to reactants.

As previewed above, the $Mu\dot{C}_6H_6$ radical is well-known, having been observed in a wide variety of different environments, and is expected also to have formed on surface-adsorbed Bz on the AuNPs in P1. In that study, the muon-spin relaxation rates, λ_{Mu}, which determined the reaction rates due to (R1), were found to scale linearly with benzene concentration in the silica mesopores, but the final-state $Mu\dot{C}_6H_6$ radical was not identified. It is the purpose of the present paper to confirm the formation of this final state interacting with AuNPs in the same mesoporous AuNP/silica samples as studied earlier and to further clarify the reaction mechanism(s) involved, via the technique of avoided level crossing (ALC) muon spin resonance.[7,11,17,22,42−46,52−58]

2. MUON SPIN RESONANCE (μSR)

2.1. Background to the Technique. Positive muons (μ^+) are produced 100% longitudinally spin-polarized, typically at a proton accelerator, TRIUMF in the present studies, and subsequently decay ($\mu^+ \rightarrow e^+ + \nu_e + \bar{\nu}_\mu$) with a mean life of 2.2 μs, in which the emitted positron, detected in the experiment, is broadcast asymmetrically along the direction of spin polarization at the time of its decay. The amplitude of the μSR signal seen, appropriately known then as the "asymmetry", depends on the energy of the detected e^+ and is generally determined empirically, as in this work. When the μ^+ slows down in matter from initial MeV to thermal energies, a large fraction can form the Mu atom by electron capture in the mesoporous silica environments of interest here, expected to thermalize to k_BT in about 1 ns, a much shorter time here in comparison with measurements in the gas phase.[59,60]

In general, μSR experiments are carried out in either a longitudinal magnetic field, along the muon spin direction (LF-μSR), or in a transverse field perpendicular to it (TF-μSR), with both incident muon and positron detection counters arranged accordingly. In TF-μSR, the muon spin precesses in the plane of these detectors, giving rise to oscillations in the observed count rate due to the asymmetric decay of the muon, as seen for the precessing Mu atom in weak TFs of a few Gauss in paper P1. In a LF geometry, with the magnetic field applied along the direction of the initial muon spin polarization, the μSR signal seen by "Forward (F)" and "Backward (B)" detectors typically shows no oscillation (there is no spin precession), but rather is described by an exponential decay characteristic of a $1/T_1$ relaxation rate. However, resonant-like features in the LF can occur at specific magnetic fields due to level crossings[22,42,50,52−56] which lead to low-frequency oscillations. The positions of these crossings provide a powerful method for investigating the electronic structure of a muoniated radical and its hyperfine coupling constants (hfcc) associated with the muon and surrounding nuclear spins. As above, this method is appropriately known as avoided level crossing (ALC) resonance spectroscopy[55,56] or just simply as level crossing resonance (LCR) spectroscopy, and it is the experimental method used herein to specifically identify the $Mu\dot{C}_6H_6$ free-radical interacting with AuNP surfaces, as depicted in reaction scheme (R1) above.

2.2. Avoided Level Crossing Resonance Spectroscopy. In the microcrystalline AuNP/silica environments here, interactions of the nuclear spin probe are anisotropic in nature, giving rise to terms in the Hamiltonian from magnetic dipole−dipole couplings,[22,51,53,55,56,58] with terms conventionally denoted A to F,

$$\begin{aligned} \hat{H} = {} & \nu_e\hat{S}_e - \nu_\mu\hat{I}_\mu - \sum_k \nu_k\hat{I}_k + A_\mu\hat{S}_e\cdot\hat{I}_\mu + \sum_k A_k\hat{S}_e\cdot\hat{I}_k \\ & - D_\mu(A^\mu + B^\mu + C^\mu + D^\mu + E^\mu + F^\mu) \\ & - \sum_k D_k(A^k + B^k + C^k + D^k + E^k + F^k), \end{aligned} \qquad (1)$$

written in frequency units. Here D_μ and D_k are the strengths of the anisotropic dipolar hyperfine interactions for the electron-muon spins ($\hat{S}_e$ is the electron spin operator with $\hat{I}_\mu$ that for the muon spin) and electron−nuclear spins ($\hat{I}_k$ are the spin operators for the protons here, k = 1−6). The Mu-cyclohexadienyl radical, like its benzene precursor, has a disk-like shape and exhibits facile rotation about its unique symmetry axis, perpendicular to the plane. This gives rise to an *axial* hyperfine tensor, with

$$D_\perp{}^\mu = -(1/2)D_\parallel{}^\mu = \frac{\gamma_e\gamma_\mu}{4\pi^2}\langle 1/r^3\rangle \qquad (2)$$

where r is the distance between the unpaired electron and the point-like dipolar nuclear spin, with components for D_μ in eq 1 given in polar coordinates[22,51,56,58] by

https://doi.org/10.1021/acs.jpcc.1c05723
J. Phys. Chem. C 2021, 125, 21410−21423

$$A^{\mu} = (1 - 3\cos^2\theta)\hat{S}_z\hat{I}_z$$
$$B^{\mu} = -1/4 \times (1 - 3\cos^2\theta)(\hat{S}_+\hat{I}_- + \hat{S}_-\hat{I}_+)$$
$$C^{\mu} = -3/2 \times (\sin\theta\cos\theta\, e^{-i\phi})(\hat{S}_z\hat{I}_+ + \hat{S}_+\hat{I}_z)$$
$$D^{\mu} = -3/2 \times (\sin\theta\cos\theta\, e^{+i\phi})(\hat{S}_z\hat{I}_- + \hat{S}_-\hat{I}_z)$$
$$E^{\mu} = -3/4 \times (\sin^2\theta\, e^{-2i\phi})\hat{S}_+\hat{I}_+$$
$$F^{\mu} = -3/4 \times (\sin^2\theta\, e^{+2i\phi})\hat{S}_-\hat{I}_-, \quad (3)$$

where θ is the angle between the unique symmetry axis of the $Mu\dot{C}_6H_6$ radical and the applied LF, and ϕ is the azimuthal angle. Note that the scalar product $\hat{S}_e\cdot\hat{I}_\mu$ for the isotropic hyperfine interaction in eq 1, can be written as $\hat{S}_z\hat{I}_z + 1/2 \times (\hat{S}_+\hat{I}_- + \hat{S}_-\hat{I}_+)$ with similar terms for the electron−proton spins, which has the same combination of operators as in A^{μ} and B^{μ} in eq 3 for the anisotropic interaction terms. As seen from eq 2, the strength D_μ is $\propto \gamma_e\gamma_\mu$, the product of electron and muon gyromagnetic ratios. Similar terms also enter for the proton−electron anisotropy, but since $\gamma_\mu = 3.184\ \gamma_p$, $D_k = D_p$ plays a smaller role.

In magnetic fields well above the hyperfine coupling field for the muoniated radical of interest (∼185 G for $Mu\dot{C}_6H_6$[7,45,46]), in the Zeeman region, the product eigenstates of muon, electron, and protons exhibit avoided level crossings, giving rise to ALC resonances at specific applied longitudinal magnetic fields.[7,22,42,50−52,56,58] This is shown in Figure 1 for a single proton,[22] which in fact is the case of interest here for the "ipso" position where Mu adds to the benzene ring, giving a methylene −CHMu group. The top part of this figure shows schematic results for the energies of this three spin ($^1/_2$) system, assuming an axial hyperfine interaction (2), labeled by their usual spin projections α and β for electron, muon, and nuclear k = proton spins.

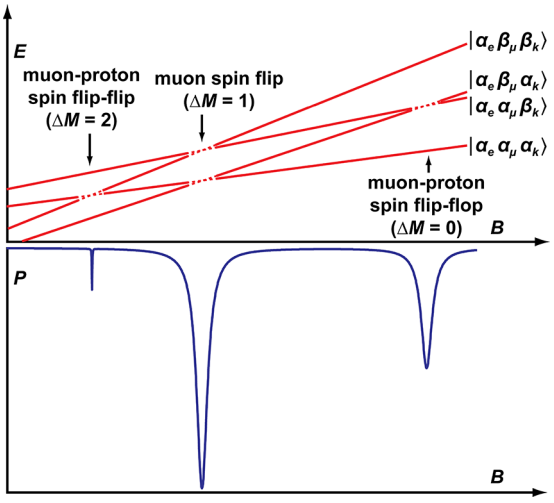

Figure 1. Schematic illustrating the nature of ALC resonances at specific applied magnetic fields for electron, muon, and nuclear (k = proton) spins in high longitudinal fields, where the eigenstates are given by product Zeeman states. The nonphysical crossings are shown as dashed sections in the above red curves, which plot the field dependence of the eigenstates for electron spin-up states (α_e), with their avoided crossings shown by the blue-line ALC Lorentzian line shapes in the bottom part of this figure. The peak amplitudes depend on the values of the isotropic hfcc for the Δ_0 lines and on the strengths of the anisotropic interactions for the Δ_1 lines. Republished with permission of the Royal Society of Chemistry, from ref 22; permission conveyed through Copyright Clearance Center, Inc.

Three distinct types of ALC resonances are seen with increasing LF in Figure 1, characterized by the change in total spin projections for fixed electron spin, α_e, $\Delta M = \Delta(m_\mu + m_p)$ between initial and final eigenstates = 2, 1, and 0, corresponding to a muon-proton spin "flip−flip", muon spin "flip" and muon-proton spin "flip-flop", respectively, all of which derive from specific terms in the Hamiltonian of eq 1. (Similar results are seen for the β_e electron spin.) Thus, for the $\Delta M = 1$ resonance, (hereafter Δ_1) the two Zeeman states $|\alpha_e\alpha_\mu\beta_p\rangle$ and $|\alpha_e\beta_\mu\beta_p\rangle$ mix in first order due to the $\hat{S}_z\hat{I}_+$ and $\hat{S}_z\hat{I}_-$ muon operators of the off-diagonal C^{μ} and D^{μ} terms in eq 3, resulting in an avoided crossing in which *only* the muon spin flips between $|\alpha_\mu\rangle$ and $|\beta_\mu\rangle$, independent of other nuclear spins. This crossing arises only from muon−electron hyperfine anisotropy[25,51−54] and so is arguably the most sensitive probe of the muon environment. For counters fixed in a longitudinal geometry, the F/B ratio changes sign on resonance, giving rise to the ALC *dip* seen for the strong Δ_1 line at midfield in Figure 1.

The upper ΔM = 0 (Δ_0) resonance shown is due to the mixing of $|\alpha_e\beta_\mu\alpha_p\rangle$ and $|\alpha_e\alpha_\mu\beta_p\rangle$ states from similar operators as $\hat{S}_z\hat{I}_+$ and $\hat{S}_z\hat{I}_-$ above, involving both the muon and proton spins simultaneously, in second order, arising from the isotropic ($\hat{S}_e\cdot\hat{I}_\mu$) *and* anisotropic ($C^{\mu}$ and D^{μ}) hyperfine interactions in eqs 1 and 3. This is the only ALC resonance that can be seen in isotropic environments, where rotational averaging of the dipolar coupling terms occurs, exemplified by studies of the $Mu\dot{C}_6H_6$ radical in the gas[45] and liquid[46] phases. There is also a very weak/narrow $\Delta M = 2(\Delta_2)$ double-quantum resonance expected, which corresponds to a muon flip−flip between states $|\alpha_e\alpha_\mu\alpha_p\rangle$ and $|\alpha_e\beta_\mu\beta_p\rangle$, also arising only in the second order but from the anisotropic muon−electron hyperfine interaction only (terms E^{μ} and F^{μ} for muon and proton in eq 3). These contribute much less than C^{μ} and D^{μ}, as seen earlier in solid benzene[7,50,51,58] and in Figure 2 here as well. Since this is such a weak line, it is only the Δ_0 and Δ_1 resonances that are of interest in the present study.

The muon "asymmetry" is a measure of its residual polarization at the time of decay, determined in a LF from the difference in positron counts in "F' and 'B" directions with respect to the muon spin. In contrast to paper P1, here it is a *time-integrated* measurement, leading to the result[58]

$$\bar{P}_z(B,\theta) = 1 - \frac{0.5q^2P_z^0}{[(\lambda^2 + q^2) + (\nu_\mu - \nu_\mu^0)^2]} \quad (4)$$

for the time-averaged polarization of the Δ_1 resonance, where

$$q = (3/2)D_\perp \sin\theta\cos\theta \quad (5)$$

for a single crystal of orientation angle θ to the LF direction, and $\lambda = \lambda' + \lambda_0$ in μs^{-1}, with λ' the relaxation rate of the on-resonance signal into a different state off-resonance and λ_0 = 0.45 μs^{-1}, the inverse of the muon lifetime. This expression represents a polarization dip of Lorentzian shape for the Δ_1 resonance (see Figures 1 and 2), with a HWHM of $[(\lambda^2 + q^2)]^{1/2}$ and with its position depending on the orientation in the field. A similar result has been derived by Kiefl,[52,53] showing also the nature of the total relaxation rate on resonance. The ΔM = 0 (Δ_0) line, a muon−proton spin flip-

https://doi.org/10.1021/acs.jpcc.1c05723
J. Phys. Chem. C 2021, 125, 21410−21423

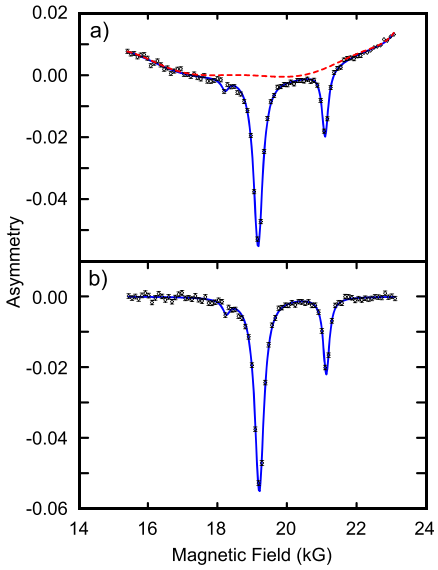

Figure 2. Experimental ALC results for bulk solid benzene at 275 K: (a) showing the background magnetic field-dependent baseline (dashed line), fit to an eighth order polynomial, revealing strong Δ_1 and Δ_0 resonances at 19.1 and 21.1 kG, respectively, seen more clearly in part b, where this background has been subtracted. In both panels, the solid lines are Lorentzian fits to the data for the Δ_1 and Δ_0 resonances of eqs 6 and 7 below, respectively. There is also a very weak Δ_2 signal at 18.2 kG, which was reproduced by a separate adjustment of the amplitude and width, since only the position could be fit. A better example of a complete fit to this weak line can be seen in ref 7.

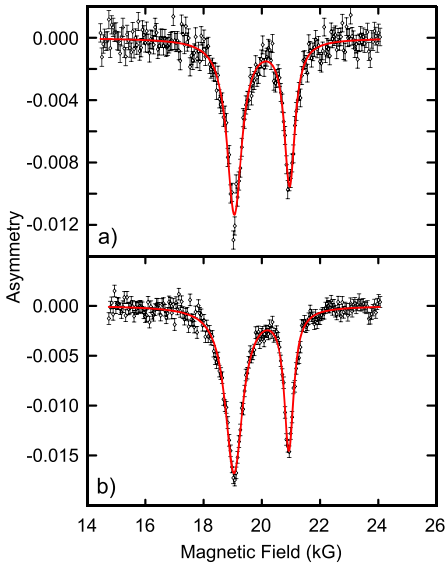

Figure 3. Background-corrected ALC scans for Bz on bare SBA-15 silica at two different loadings, 30 Torr (a) compared with 60 Torr Bz (b) at 300 K. These, and similar loadings that follow, were delivered as vapor from a "standard volume" (SV) vessel on the gas-handling system, explained in paper P1.

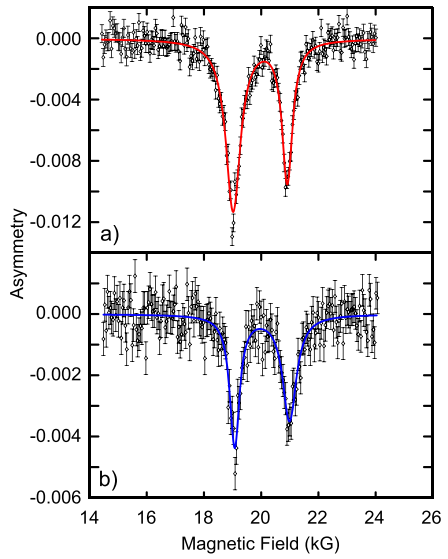

Figure 4. ALC plots for 30 Torr of added Bz from a SV ($\sim 1.4 \times 10^{-5}$ mol of Bz) on bare SBA-15 silica, taken from Figure 3 (a, red points and fitted line), contrasted with the same loading in an 8 nm AuNP/silica sample, also at 300 K (b, blue points and fitted line), corresponding to about 2−3 monolayers on the AuNP surface were they to be lying flat. See also caption to Figure 2. Note the much larger peak amplitudes in the bare silica (top) for both the Δ_1 and Δ_0 resonances at the lower and higher fields, respectively, compared to those in the AuNP sample, as well as the narrower Δ_1 resonance seen on the AuNP surface compared to the silica. See entries in Table 1. Such spectra typically take about 2 h to accumulate.

flop transition, also of Lorentzian line shape, but allowed only in second order,[54,58] is generally expected to be weaker than the first-order Δ_1 line, as seen for the higher-field lines in Figures 1 and 2 with peak amplitudes that are specifically dependent on the widths in a particular environment.

The results for the $D_\perp$ and $D_\parallel$ components of an axial hyperfine interaction in eq 2 already imply the existence of some motional dynamics averaging a more generalized anisotropic hyperfine interaction. In addition, the present studies of the $Mu\dot{C}_6H_6$ radical have mainly been carried out in SBA-15 silica *powder*, giving rise to a superposition of resonant fields that correspond to different possible orientations of the angle dependence shown in eqs 3, since the hfcc for both the muon and nuclear spins are angle dependent. Such powder-averaged line shapes typically deviate from symmetric,[42,56−58] depending on the value of λ' noted above, the degree of hyperfine anisotropy and on the angle of rotation either about the symmetry axis for an axial hyperfine tensor, $D_\parallel$, or perpendicular to it, $D_\perp$, from eq 2. See also Figure 3 in ref 56. We have not carried out such averages in the present work, but instead we have fit the experimental ALC signals seen in Figures 2−7 that follow to phenomenological Lorentzian line shapes, guided in part by eq 4 but mainly by the observation of their symmetric line shapes for both the Δ_1 and Δ_0 resonances. See also discussion in ref 7. It transpires that it is the *amplitudes* of these fitted lines that are most relevant here.

3. ALC EXPERIMENTAL RESULTS

Figure 2 shows an ALC spectrum for bulk solid benzene from the present study at 275 K. The upper panel (a) shows the "raw" data, exhibiting a field-dependent background arising from the effect of the magnetic field focusing the muon beam as well as affecting the positron trajectories. This was fit to an eighth order polynomial (red dashed line), as in all the cases that follow. Subtracting this background (b) shows the same two strong resonances expected from the schematic in Figure 1, a Δ_1 line for the muon at ∼19 kG (Table 1) and a Δ_0 for the proton at ∼21 kG. However, though bulk benzene forms a single crystal in the solid[7,51,58] that is not accounted for in the

https://doi.org/10.1021/acs.jpcc.1c05723
J. Phys. Chem. C 2021, 125, 21410−21423

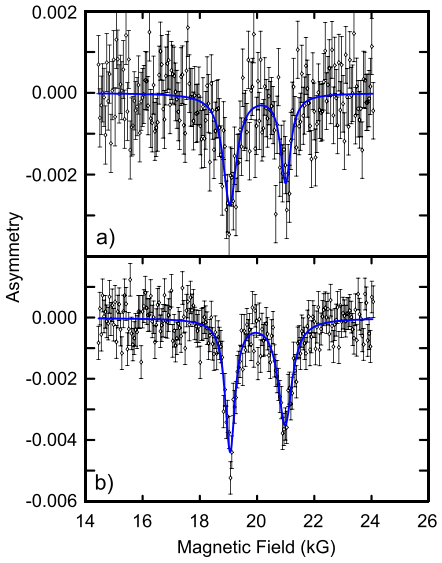

Figure 5. Background-corrected ALC scans for a nominal monolayer (or, possibly, submonolayer; see P1) of 7.6 Torr Bz on an 8 nm AuNP/silica sample (a) at 300 K, compared with a loading of 30 Torr Bz (b), the same as seen in Figure 4. See caption to Figure 2. Note that the peak amplitudes are higher at the higher loading, and note as well that the sample morphologies are the same in both cases here.

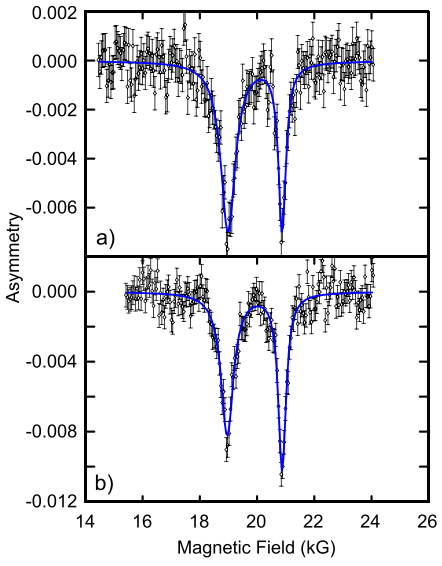

Figure 6. Background-corrected ALC scans for a loading of 83 Torr Bz/SV on the 10 nm AuNP sample (a), corresponding to ∼5 monolayers, were they to be lying flat; (b) same as in part a but for a loading of 208 Torr. Both spectra were obtained at 305 K. Similar plots are seen for other loadings with results given in Table 1.

phenomenological fits shown in Figure 2. The ratios of peak amplitudes in Figure 2 just happen to be similar to those plotted in the schematic shown in Figure 1.

The Δ_0 resonances for $Mu\dot{C}_6H_6$ here are for the "ipso" proton at the C(6) site where the Mu atom adds to the ring.[45,46,58] Weaker Δ_0 resonances for the ortho and para protons have been reported elsewhere,[7,45,46] but they are not explored here. Although certainly weak, as in the schematic of Figure 1, the Δ_2 resonance can be seen at ∼18.2 kG in Figure 2 for solid Bz, first studied by Roduner,[51,58] and as part of a later study of the MuC_6H_6 radical in the zeolite "supercages" of

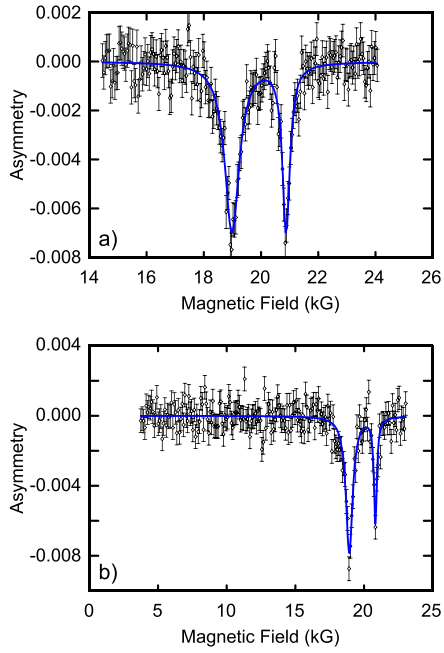

Figure 7. Comparison of background-corrected ALC scans near 300 K for a loading of 83 Torr Bz on the 10 nm AuNP sample (a, taken from Figure 6), with the same loading but scanned down to 4 kG (b), revealing no further resonances. Note the dramatic change in the *x*-axis scale for the field scan in this case (panel b). A similar outcome was found for a loading of 21.5 Torr Bz on this AuNP.

NaY, HY, and USY zeolites in ref 7. Noteworthy from ref 7 is that, just above its melting point of 279 K, the Δ_1 and Δ_2 resonances disappear in bulk benzene due to the transition to the isotropic environment of the liquid. However, the Δ_1 line remains clearly visible above the bulk benzene melting point in the silica mesopores of the SBA-15 samples in the present study (Figures 3−6), as was the case for $Mu\dot{C}_6H_6$ in the zeolite supercages of ref 7.

ALC results for *bare* SBA-15 silica are shown in Figure 3 at a loading of 30 Torr benzene (a), compared with a 60 Torr benzene (Bz) loading (b). The positions of both the Δ_1 and Δ_0 resonances and hence their hfcc are essentially the same as those in solid benzene (Figure 2). Noteworthy are the *amplitudes* of the ALC signals seen here, as measured by their peak intensities, which qualitatively scale linearly with Bz loading (Table 1, Figure 9 below), and which are much larger than those seen in the AuNP/silica samples. In a previous study of $Mu\dot{C}_6H_6$ in the siliceous zeolites, HY and USY,[7] it was assumed that the muoniated radical was weakly interacting with hydroxyl (−OH) groups in the zeolite supercages. That is also expected to be mainly the case in the SBA-15 silica here, consistent with the elemental analysis discussed in paper P1. In the more restricted environment of these silica mesopores, surface roughness[61,62] on the walls may also be playing some role, serving as trapping sites for either the AuNPs or added Bz. Even so, we would not expect any appreciable differences in hfcc for $Mu\dot{C}_6H_6$, in accord with the two distinct ALC resonances consistently seen (Figures 3−6).

At a representative loading of 100 Torr Bz (Table 1), there are $\sim 5 \times 10^{18}$ Bz molecules in the sample cell, compared to $\sim 10^{22}$ possible SiO_2/SiOH binding sites in either the bare silica or AuNP/silica samples, so some 2×10^3 more silica sites than Bz molecules at such loadings. There is little chance then of multiple benzenes at a silica site, in contrast to the case for

https://doi.org/10.1021/acs.jpcc.1c05723
J. Phys. Chem. C 2021, 125, 21410−21423

Table 1. Positions, B_r, and hfcc A_μ and A_p, for the Δ_1 Resonances of the $Mu\dot{C}_6H_6$ Radical, along with Their Peak Heights and Widths for Different Benzene Loadings, near 300 K

sample	pressure (Torr)[a]	B_r (kG)[b]	A_μ (MHz)[c]	A_p (MHz)[d]	peak height, Δ_1[e]	width, Δ_1[e] (G)
SBA-15 + Bz	30 (∼14)	19.044	518.6 ± 0.2	127.2 ± 0.3	0.011 ± 0.001	740 ± 40
SBA-15 + Bz	60 (∼28)	19.029	518.2 ± 0.2	127.1 ± 0.2	0.019 ± 0.001	840 ± 34
solid Bz, 275 K	–	19.172	522.1 ± 0.2	127.7 ± 0.2	0.055 ± 0.006	360 ± 8
8 nm AuNP + Bz	7.6 (∼3.5)	19.034	518.2 ± 0.5	126.1 ± 1.2	0.0028 ± 0.0010	670 ± 200
8 nm AuNP + Bz	15 (∼7.0)	19.029	518.2 ± 0.5	126.6 ± 0.7	0.0040 ± 0.0008	540 ± 60
8 nm AuNP + Bz	30 (∼14)	19.045	518.6 ± 0.4	126.8 ± 0.6	0.0044 ± 0.0006	480 ± 65
10 nm AuNP + Bz	21.5 (∼10)	19.058	519 ± 0.8	128.4 ± 1.2	0.0025 ± 0.0010	610 ± 220
10 nm AuNP + Bz	83 (∼38.5)	18.971	516.6 ± 0.4	126.6 ± 0.4	0.0072 ± 0.0010	720 ± 80
10 nm AuNP + Bz	115 (∼53.5)	18.966	516.5 ± 0.3	126.6 ± 0.3	0.0090 ± 0.0008	680 ± 56
10 nm AuNP + Bz	208 (∼96)	18.939	515.7 ± 0.3	125.8 ± 0.4	0.0106 ± 0.0011	760 ± 68

[a]Pressure of added Bz from the SV of ∼8.7 mL, let into the previously evacuated target cell, as described in ref 5, paper P1. The corresponding estimated numbers of μmoles of loaded Bz are given in parentheses, also from P1. [b]Fitted positions at the field minima of the Δ_1 resonances seen in Figures 2−7, errors $\lesssim$0.04 G. [c]The muon hfcc determined from the Δ_1 resonances, eq 6. [d]The "ipso" proton hfcc determined from from the Δ_0 resonances, eq 7. [e]The peak amplitudes and widths (fwhm) for the Δ_1 resonances from the eighth order background polynomial fits shown. From a 10th order polynomial fit to the background, systematic errors expected to be ∼20% for the amplitudes and 10% for the widths.

the 8 and 10 nm AuNPs, where there are only $\sim 10^{16}$ NP sites present (see paper P1). Given that there are many more silica binding sites than Bz molecules, a linear dependence on Bz loading for $Mu\dot{C}_6H_6$ formation at these sites would be expected, as seen in Figure 9 below. The large ALC amplitudes for the bare silica seen in Figure 3 also indicate that the added benzene is well distributed throughout the silica sample volume.

The ALC results for 30 Torr Bz in the bare SBA-15 silica from Figure 3 are compared with the *same* loading in the 8 nm AuNP/silica sample in Figure 4. Both environments show the same two strong resonances for $Mu\dot{C}_6H_6$ at essentially the same positions as in bulk benzene (Figure 2) and bare silica (Figure 3), and thus exhibit the same hfcc (Table 1), a result seen throughout this work. This insensitivity of muon hfcc to binding sites is a well-known result from past studies of $Mu\dot{C}_6H_6$ in different environments,[7,13,41,42,45,46] testifying to its generally weak interaction in these environments, including Comment/Request: please do not split up the formula for MuC6H6 at the end of the line above with the AuNPs herein. Thus, the measured hfcc (A_μ and A_p in Table 1) also do not differ by much more than 1% from previously established values, reflecting the resonance stability arising from electron delocalization via C=C bond conjugation in both the precursor Bz and the muoniated radical formed in (R1).

In Figure 4, though the hfcc for $Mu\dot{C}_6H_6$ do not differ between the bare silica and 8 nm AuNP/silica sample, there are differences in both the widths and particularly in the peak amplitudes, as shown for the Δ_1 resonances from all scans listed in Table 1. Thus, while the Δ_1 resonance for $Mu\dot{C}_6H_6$ in the AuNP sample (Figure 4b) is somewhat broader than in the bulk (Figure 2), this broadening is seen much more dramatically in the bare silica (Figure 4a), which is twice as broad as in the bulk or in this 8 nm AuNP sample, indicative of a weaker interaction energy between $Mu\dot{C}_6H_6$ at silica sites than at AuNP sites, in accord as well with the measured relaxation rates, λ_{Mu}, in paper P1. This led to our proposal in P1, and supported herein, that the added Bz and hence the $Mu\dot{C}_6H_6$ radical was primarily located *on* the AuNPs, *not* at the vastly more abundant silica sites in the AuNP/silica samples, due to the expected stronger BE of Bz to the AuNPs. The weaker interaction energy of $Mu\dot{C}_6H_6$ with mainly −OH sites in the bare silica could give rise to more motion of the free radical at those sites, possibly sampling then extended regions of hyperfine anisotropy[25] and thus contributing to the increased line broadening noted. It is noteworthy here as well that, were $Mu\dot{C}_6H_6$ located at silica sites in the AuNP/silica sample, we would expect to see widths similar to those in Figure 4a), contrary to observation in Figure 4b). See also Figure 8 below.

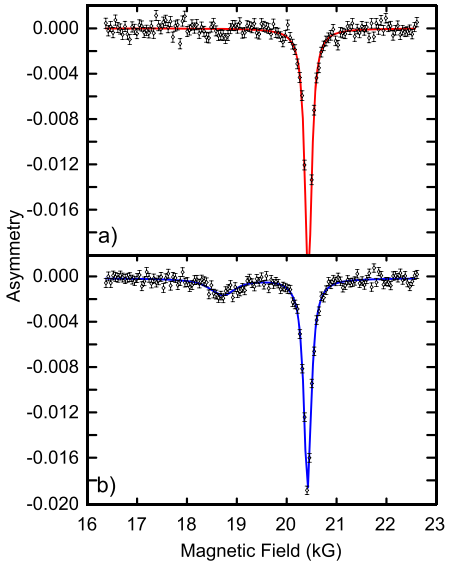

Figure 8. Comparison of a bare SBA-15 sample at a high Bz loading of $\sim 10^{-4}$ moles of Bz at 418 K (a) with the same loading on a 30 nm AuNP in a AuNP/silica sample at 418 K (b). Adapted from ref 11. For reference, the highest loading in the present study (Table 1) is comparable. Note the loss of the Δ1 resonance in the upper scan for the bare silica, but which, though highly broadened, is still clearly seen in the fit for the AuNP data in part b.

The $\sim 10^{22}$ possible SiO_2/SiOH binding sites in either the bare silica or AuNP/silica samples are also some 10^6 times larger than the number of AuNP sites estimated in P1, in accord with multiple benzenes expected to be present at these sites, and hence with the reduced amplitudes of the ALC signals seen for the 8 nm AuNP/silica sample in Figure 4 compared to the bare silica. The peak heights for both resonances (listed for the Δ_1 in Table 1), are about 3 times *less*

https://doi.org/10.1021/acs.jpcc.1c05723
J. Phys. Chem. C 2021, 125, 21410−21423

for the AuNP sample at this 30 Torr Bz loading, likely due to the formation of *diamagnetic* final states on the AuNP surfaces,[3,5] for which there is no clear route were $Mu\dot{C}_6H_6$ located at SiO_2/SiOH sites. Were Bz to be located at silica sites in the AuNP/silica samples, little or no difference in ALC amplitudes would be expected, contrary to the observation in Figure 4.

Though hyperfine anisotropy, molecular reorientation, and powder-averages can give rise to asymmetric ALC line shapes for muoniated free radicals, from which their molecular dynamics can be assessed,[17,22,42,51,54,56,57,63] the Δ_1 and Δ_0 resonances seen here are well described by the phenomenological/symmetric Lorentzian fits shown in Figures 2−7, giving the field positions $B_r(\Delta_1)$ and $B_r(\Delta_0)$. These in turn give the isotropic hfcc, A_μ for the muon, from the minimum of the Δ_1 resonance, and A_p for the proton from the Δ_0 resonance, found from eqs 6 and 7, respectively:

$$B_r(\Delta_1) = \frac{1}{2}\left|\frac{A_\mu}{\gamma_\mu} - \frac{A_\mu}{\gamma_e}\right| \tag{6}$$

$$B_r(\Delta_0) = \frac{1}{2}\left|\frac{A_\mu - A_p}{\gamma_\mu - \gamma_p} - \frac{A_\mu + A_p}{\gamma_e}\right| \tag{7}$$

with the gyromagnetic ratios γ_μ = 0.01355 MHz/G and γ_e = 2.8025 MHz/G. The reduced denominator in the first term of eq 7 indicates that the position of the Δ_0 resonance will typically be *above* the Δ_1 for most organic free radicals, seen in the schematic of Figure 1 and in all the experimental ALC plots for $Mu\dot{C}_6H_6$ here and elsewhere.[7,42,45,46,58] In both eqs 6 and 7, the first terms arise from the crossing of the energies shown in Figure 1, but which are avoided in the presence of hyperfine anisotropy,[22,52−54,56,58] due to off-diagonal matrix elements in the Hamiltonian of eq 1. It follows then that the very observation of a Δ_1 resonance here means that the $Mu\dot{C}_6H_6$ radical cannot be isotropically rotating within the SBA-15 mesopores, but rather its motion is rotationally hindered due to being localized at specific binding sites. This may be the case as well in a recent neutron scattering study of Bz located in the mesopores of MCM-41 silica,[64] recognizing that the pore sizes of ∼1.8 nm are much smaller than those of interest here in SBA-15 silica.

It should be noted that there is a difference in the measurement time scales involved in our earlier P1 paper and for the ALC results here. In the weak TF-μSR study of P1, the spin-dephasing relaxation (λ_{Mu}) of Mu with surface-adsorbed Bz on the AuNPs in the mesopores had to be fast compared to other spin-relaxation effects, and notably faster than electron spin-exchange (SE) due to paramagnetic impurities or "dangling bonds" arising from the synthesis procedure. It was also pointed out in P1 that differences in sample morphology could affect the volume of the mesopores differently for the bare silica and AuNP/silica samples, giving different concentrations of benzene, which could then directly affect the measured relaxation rates, λ_{Mu}, in P1.

In an ALC experiment though, carried out in high LFs, there is no coherent spin precession and hence no dephasing. There is no SE for Mu on the MHz time scale seen in paper P1 either, since at the high LFs utilized to give the ALC signals of interest here, any such SE would be completely quenched; hence the amplitudes of the ALC signals can develop over the much longer 2.2 μs lifetime of the muon. Thus, λ_{Mu}, due to the chemical addition rate described by (R1), need only be $\gtrsim \sqrt{\lambda^2 + q^2}$ for the HWHM in eq 4 in order to guarantee a large transfer of the muon polarization to the radical. From the entries for the widths of the AuNP/silica samples in Table 1 below, though not single crystal environments, this condition would appear to be, by and large, well satisfied, so any differences in sample morphology on the ALC amplitudes for the AuNP samples in the present study are expected to be of less concern than was the case for the reaction rates discussed in P1.

There is another important aspect here, relating to the resonance stability of the cyclohexadienyl radical. Though the measured muon hfcc, A_μ, for $Mu\dot{C}_6H_6$ in a variety of different environments[7,17,45,46,58] are all within about 1% at a given temperature, seen also here from the results in Table 1, that was not the case for $Mu\dot{C}_6H_6$ in NaY zeolite, which *strongly* interacts with the Na^+ cations,[7] markedly distorting the cyclohexadienyl radical from its normal planar geometry, causing 20% shifts in A_μ for inequivalent C−Mu bond orientations, above ("exo", + 20%) and below ("endo", −20%) the plane. In contrast, $Mu\dot{C}_6H_6$ in the siliceous zeolites, USY and HY, in the same study, interacts only *weakly* with mainly framework −OH groups, leaving a largely planar radical with values for A_μ that are again within ∼1% of those seen in bulk benzene.[7] That is the case in the ALC study here as well, comparing solid benzene (Figure 2), bare silica (Figure 3), and the AuNP/silica samples (Figures 4−6), in accord also with the analysis in P1, where Bz was also found to be weakly interacting with the AuNPs. The muon hfcc *do not* then provide any indication of site location for the $Mu\dot{C}_6H_6$ radical between SiO_2 and AuNP sites in the present study, in contrast to their peak amplitudes discussed below.

Since there are $\sim 2 \times 10^3$ more SiO_2 sites than benzenes at typical loadings, there are also then some 10^3 times *fewer* AuNPs than benzene molecules; hence, several benzenes can be accommodated at AuNP sites given that a typical size for a benzene molecule is ∼0.5 nm, much less than the AuNP size. Benzene consequently adopts a *canted* orientation on the AuNP surface, explaining the linear dependence of λ_{Mu} on [Bz] seen in P1. This also facilitates Mu reactivity with bare AuNP sites forming *diamagnetic* final states[3,5] due to its chemisorption at these sites, as a possible probe of surface magnetism, in sync with a more recent paper elsewhere.[65]

Figure 5 compares ALC spectra for $Mu\dot{C}_6H_6$ on the 8 nm AuNP at an expected monolayer loading of 7.6 Torr Bz (a) with the 30 Torr Bz loading from Figure 4 (b), while Figure 6 compares results for two higher Bz loadings in the 10 nm AuNP/silica sample. These spectra show the same two strong Δ_1 and Δ_0 resonances in both environments, as in Figures 2−4, hence with the same hfcc (Table 1). The peak amplitudes of both resonances are consistently lower though at the lower loadings. That the Δ_1 resonances are clearly visible near 300 K in both the silica and AuNP environments (Figures 3−7), in contrast to bulk benzene at temperatures just above its melting point,[7] could be indicating an effect of the constricted environments of the silica mesopores on the melting points and dynamics of benzene and the $Mu\dot{C}_6H_6$ radical within these mesopores.[47,66−70]

Though the positions of these ALC resonances are insensitive to $Mu\dot{C}_6H_6$ binding sites, their amplitudes are not. Even at the higher loading of 83 Torr in Figure 6a, compared to the similar loading of 60 Torr in bare silica in

https://doi.org/10.1021/acs.jpcc.1c05723
J. Phys. Chem. C 2021, 125, 21410−21423

Figure 3b, the peak amplitudes in the silica are still almost 3 times higher, indicating a chemisorption reaction of Mu with the AuNPs forming a diamagnetic final state,[3,5] thus reducing the ALC amplitudes seen. There is a difference in the widths on the 8 nm AuNP at 30 Torr Bz in Figure 5b, which is narrower than for both the 10 nm AuNP and the bare silica at comparable loadings (Figure 3a, Table 1), indicating a stronger BE for $Mu\dot{C}_6H_6$ to the smaller AuNP. Both the differences in widths and peak amplitudes seen for the ALC resonances in Figures 5 and 6, and given in Table 1, compared to those in bare silica, support the claim herein (and for benzene in P1) that the MuC_6H_6 radical is indeed *weakly* interacting with AuNP sites, and is not located at silica sites in these AuNP/silica samples.

Were that not the case, and the $Mu\dot{C}_6H_6$ radical was strongly interacting with the AuNPs, additional delocalization of the unpaired electron compared to that for an isolated radical in the bulk[7,13] would be expected to give rise to a reduced overlap with the muon in the C−Mu bond of the radical and hence to a reduced muon hfcc, A_μ, meaning a shift in the positions of both the Δ_1 and Δ_0 resonances to lower fields. This prompted ALC studies down to 4 kG (and below), seeking evidence for such a possibly reduced hfcc, as shown by the scan in Figure 7b. However, no additional resonances were seen, in accord with the view herein and in P1 that benzene, canted on the surface and the $Mu\dot{C}_6H_6$ radical so formed in (R1), interacts only weakly with the AuNP surfaces, expected as well from the general stability of this muoniated radical.

Figure 8 shows results for the $Mu\dot{C}_6H_6$ ALC resonances from a separate study[11] on a 30 nm AuNP at a relatively high Bz loading of $\sim 10^{-4}$ mol at a temperature of 418 K, compared with the same loading on a bare SBA-15 silica sample. The Δ_1 resonance on the AuNP, though highly broadened due to the desorption and molecular motion of $Mu\dot{C}_6H_6$, is still clearly visible in the lower scan (b), but for the bare SBA-15 sample, this resonance has broadened to such an extent that it has disappeared into the background (a), an outcome seen also at lower temperatures.[11] The clear difference seen in the ALC peak heights between the bare silica and AuNP samples at 418 K in Figure 8 echoes the claim above that the $Mu\dot{C}_6H_6$ radical is preferentially interacting with the AuNPs as opposed to being located at silica sites in these Au/SBA-15 samples; otherwise there would be no difference seen in these spectra.

4. DISCUSSION: MECHANISMS AND THE $MU\dot{C}_6H_6$ FINAL STATE

The reaction of Mu to form the $Mu\dot{C}_6H_6$ radical causes a relaxation rate of the Mu precession signal, λ_{Mu}, that was studied on both bare silica and AuNP/silica samples of different NP sizes in P1. There are only two distinct sites for the location of this radical: at bare silica sites or at AuNP sites. Since the BE of Bz is expected to be stronger to AuNPs than to SiO_2/SiOH sites, despite their greater number, it was reasonable to propose (P1) that most of the added benzene would be located on the AuNPs, giving rise to a linear dependence of λ_{Mu} on [Bz], in accord with the Eley−Rideal model of surface reactivity discussed in P1. Such a dependence is in marked contrast to an asymptotic trend that would have been the case were Bz, at multilayer loadings, lying flat on the NP surface, like "stacked dinner plates" due to π-stacking interactions.[5,71] This linear dependence seen for λ_{Mu} in paper P1 resulted from the weak interaction of Bz with the AuNPs and its *canted orientation* on the NP surfaces, allowing for many more bare AuNP sites as well as more Bz surface-adsorbed sites for Mu to react with than would have been the case were Bz lying flat. Still, one cannot exclude the possibility that some Bz and hence some $Mu\dot{C}_6H_6$ radicals could also be located at silica sites, in the face of the uncertainties in sample morphologies discussed in P1.

It is worthwhile to briefly review here what led us to propose this canted orientation of benzene on the AuNPs in P1. On a planar metal surface, and in particular for Bz on a Cu(110) surface[72] discussed in P1, the BE of Bz to the metal was believed to be stonger than to a AuNP surface, thus forming a monolayer lying flat on the metal surface; but that is not necessarilly the case for the AuNP surface. Lee et al.[72] showed that successive Bz multilayers on the Cu(110) surface were oriented on an initial monolayer in an "edge-on" geometry, which we suggested could also be the case for Bz at some "canting" angle to the AuNP surface in P1. However, not as multilayer loadings but more likely as individual benzenes (or perhaps small clusters) on the AuNP surface, given their expected weaker BE compared to an extended metal surface and the constricted geometry of the SBA-15 mesopores; in accord as well with the observed linear dependence on Bz concentration seen in the relaxation rates λ_{Mu} in P1. (Such a canting effect has also been reported in ref 64 for benzene encapsulated in the even more restricted pores of MCM-41 silica.)

A canted Bz precursor on the AuNPs is also presumed to give similarly oriented $Mu\dot{C}_6H_6$ radicals on the AuNP surface from (R1), each one behaving in like manner to its neighbor, in accord with the similar positions for the ALC resonances seen in Figures 4−6 and hence with the similar values for the hfcc found (Table 1); also a consequence of the resonance stability of the Bz precursor and the $Mu\dot{C}_6H_6$ radical that is formed, both weakly interacting with the AuNP surfaces.

Electron SE, mentioned above, requires additional comment here. This was explored in P1 as a competitive process contributing to λ_{Mu}, along with the dephasing caused by the chemisorption reaction of Mu forming a diamagnetic final state on the AuNP surfaces.[3,5] This SE effect was not seen in all AuNP samples though and moreover was quenched in moderate longitudinal magnetic fields, indicative of "slow SE" due to paramagnetic impurities arising from the synthesis processes in making the AuNP/silica samples. On the other hand, were this to have happened on a much faster time scale for the $Mu\dot{C}_6H_6$ radical *in contact with* the AuNP surface, a strong damping of the muon polarization in the final state would have been seen, leading to excessive broadening of the ALC lines.[56] Since this is not observed (Table 1), we propose that the unpaired electron of the muoniated cyclohexadienyl radical is *not* in direct contact with the metal surface. Such a fast relaxation effect is seen in ref 18 though, on the interaction of stable nitroxyl radicals with AuNPs in solution, giving no EPR signals, attributed to rapid SE of the unpaired radical electron in contact with the conduction electrons on the AuNP surface.

The μSR technique utilized to establish the linear dependence of λ_{Mu} on [Bz] seen in P1 was sensitive only to the *initial* state of the system in reaction (R1). This did suggest though that a similar dependence could be expected for the amplitudes of the ALC resonances for the *final* free radical $Mu\dot{C}_6H_6$ state formed, since this could be expected to scale qualitatively with λ_{Mu}. However, that was found to not be the case, as the results for the peak amplitudes of the Δ_1 resonances for the AuNP

https://doi.org/10.1021/acs.jpcc.1c05723
J. Phys. Chem. C 2021, 125, 21410−21423

samples listed in Table 1 and plotted vs Bz loading in Figure 9 clearly show, particularly for the 10 nm AuNP/silica sample which covers the widest range of Bz loading. Similar trends were seen for the Δ_0 resonances.

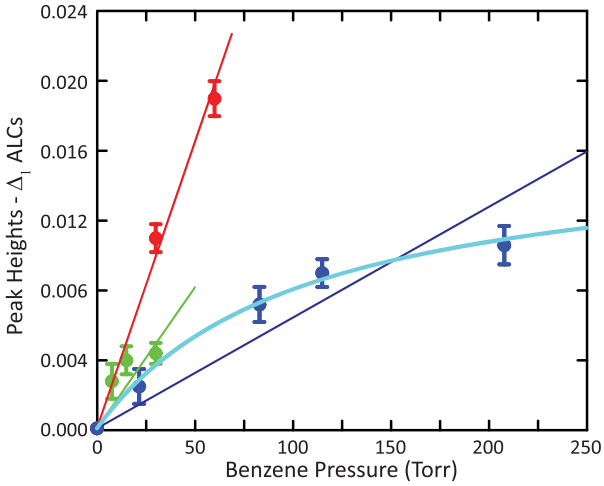

Figure 9. ALC peak heights for the Δ_1 resonances for the bare SBA-15 silica (red points and linear fit), 8 nm AuNP (green points and linear fit) and 10 nm AuNP blue points and linear fit) vs the SV pressure of added benzene from Table 1. See footnote e in Table 1. The cyan-line is a fit to an asymptotic dependence for the 10 nm AuNP, from eq 8 in the text. It is noted that this trend is not predicated on the data point at the highest Bz pressure of 208 Torr. All data were obtained at 300 K.

It is worth echoing an earlier point here that, though the ALC peak positions (and hence hfcc) in Table 1 do not change with Bz loading, their peak intensities *do* change, and quite dramatically so in comparison with those for the bare silica, by as much as a factor of 10 at an (extrapolated) loading of 250 Torr in Figure 9. A similar trend is seen for the 8 nm AuNP size up to lower loadings (green points). For both of these cases the dependence on the added Bz pressure was measured in the same sample cell for the same beam conditions, thereby minimizing possible systematic variations in the measured ALC amplitudes due to different muon beam-spot sizes or stopping distributions. As noted earlier (footnote e, Table 1), these amplitudes are relatively insensitive to changes in polynomial background fits. The changes in intensity seen in the ALC signals for the AuNP/silica samples in Figure 9 are thought to be due to the formation of hidden *diamagnetic* final states, either from Mu reacting with bare AuNP surfaces,[3,5] in competition with $Mu\dot{C}_6H_6$ formation, expanded on in (R2) below, or possibly via a rapid transfer of the unpaired electron of the radical from the intermediate $Mu\dot{C}_6H_6^*$ state to the metal surface, leaving a $MuC_6H_6^+$ diamagnetic final state, explored in (R3) below.

It is remarked that, if an initial monolayer of Bz were formed, lying flat on the AuNP surface, as suggested early on in ref 11, such a layer could shield the underlying metal from subsequent benzenes, which would then interact via Bz···Bz physisorption as opposed to Bz···AuNP chemisorption, also giving then hfcc that would not change with Bz loading. However, such a model would give as well no change in ALC amplitudes with Bz loading, contradicting the change seen in Figure 9 as well as the linear dependence seen for λ_{Mu} on [Bz] in P1.

For $Mu\dot{C}_6H_6$ bound at silica sites in the *bare* SBA-15 silica (red line) in Figure 9, there are only two data points, but the intercept at [Bz] = 0 also determines the fit, which does seem then to be clearly linear, as assumed in Figure 9. Since there are $\sim 10^6$ times more SiO_2 than AuNP sites, a similar linear dependence as seen by the red line would be expected were $Mu\dot{C}_6H_6$ located at SiO_2 sites in the 8 and 10 nm AuNP/silica samples. Linear fits to these data are shown by the green and blue lines, respectively, both having much shallower slopes than seen for the bare silica. Though this linear fit for the 8 nm AuNP sample could be deemed satisfactory, given the few closely spaced data points, the linear fit for the 10 nm AuNP, indicating an even shallower slope, *fails* completely to account for the trend seen in the Δ_1 amplitudes, given also that this covers ten times the range in Bz loading. These observations provide additional support for our claim herein (and in P1) that the added Bz is mainly located *on/at* the AuNPs.

The extended trend for the 10 nm AuNP/silica data in Figure 9 indicates an asymptotic dependence, which can be described by the phenomenological expression

$$\mathrm{Amp}(\Delta_1) = \frac{A_1 + A_2 \times P}{(A_3 + 0.2P)} \tag{8}$$

similar to that explored in P1 (see Figure 10 therein), with parameters A_1, A_2, and A_3, shown by the cyan-fitted line to the 10 nm AuNP data in Figure 9, giving a much better fit than a linear dependence. The pressure P here is given in Torr, and the values of the fitted parameters are 1.0×10^{-4}, 3.2×10^{-3} ,and 20.9 Torr for A_1, A_2 and A_3, respectively, the latter indicating the onset of quite a strong damping of the amplitude even at low pressures. (The constant factor of 0.2 in the denominator of eq 8 is fixed, given the few data points; choosing a similar but different value made little or no difference in the fit.) Though not shown, eq 8 also gives a better fit to the 8 nm AuNP/silica data than the linear (green line) fit shown, despite its more closely spaced data points.

There are only a few reports relating to metal NP stability, catalytic activity and energy transfer with surface-adsorbed molecules in general[20,67,73−76] and for the interaction of free radicals with bulk metal or metal NP surfaces in particular. As noted above, an ESR study of a stable nitroxyl radical in contact with gold NPs in solution showed no signal,[18] attributed to rapid SE between its unpaired electron and the electrons on the NP surface, though this could also be interpreted as due to a rapid loss of that unpaired electron to the metal. Earlier examples are that of Carley et al., who detected the hydrogenated radicals $HCH_2\dot{C}H_2$ and $H\dot{C}_6H_6$ on a silica-supported Pd catalyst by ESR,[16] and by Schwager et al. for the $Mu\dot{C}_6H_6$ radical in the same system,[13] commented on further below. The cyclohexadienyl ($H\dot{C}_6H_6$) radical was also detected by ESR in MCM-41 zeolite due to H-atom addition to benzene.[15]

Since the asymptotic trend seen in Figure 9 for the peak heights of the Δ_1 resonances on the AuNPs is thought to be due to the underlying formation of unobserved diamagnetic final states,[3,5] we seek mechanisms in accord with that view, going beyond the basic reaction scheme of (R1) above. The most straightforward extension for this is given by (R2), reflecting as well the theme of recent results reported elsewhere.[65] Thus, in competition with $Mu\dot{C}_6H_6$ formation,

https://doi.org/10.1021/acs.jpcc.1c05723
J. Phys. Chem. C 2021, 125, 21410−21423

$$\mathrm{Mu} + \mathrm{AuNP}/\mathrm{C_6H_6} \rightarrow \underset{\mathrm{H_6{\cdot}AuNP}\uparrow}{\mathrm{Mu\dot{C}_6H_6^*{\cdot}AuNP}} \xrightarrow{[f,\ k_S]} \mathrm{MuC_6H_6{\cdot}AuNP}\uparrow \xrightarrow{[(1-f),\ k_C]} \mathrm{Mu}\cdots\mathrm{AuNP} + \mathrm{C_6H_6}, \quad \text{(R2)}$$

where, as in (R1), a stabilized $\mathrm{Mu\dot{C}_6H_6}$ radical could be formed on the AuNP surface (with the ↑ indicating its canted orientation (not to be confused with the use of this same arrow to indicate the direction of the muon spin in P1), with branching ratio "*f*", and Mu···AuNP signifies the formation of a diamagnetic final state, determined by the rate constant k_C, in a similar manner here to that for chemisorbed Mu.[3,5] While it cannot be ruled out that some $\mathrm{Mu\dot{C}_6H_6}$ might also be localized at bare silica sites, in that case though there would be no clear mechanism for the formation of diamagnetic final states. With increasing Bz loading, there are fewer bare AuNP sites and thus $f \rightarrow 1$, as seen by the cyan-line fit to the 10 nm AuNP data in Figure 9.

The ALC signals shown in Figure 5 for the 8 nm AuNP/silica sample are instructive here. Panel a shows results for a nominal monolayer loading (or less) of 7.6 Torr Bz. Taken at face value, this raises an important question: why are there any ALC signals seen at all at such a low loading on this metal NP surface? One would expect the $\mathrm{Mu\dot{C}_6H_6}$ radical, *if* in direct contact with the metal NP, to either rapidly lose its unpaired electron to the metal, giving then an anticipated 100% diamagnetic signal from both the $\mathrm{MuC_6H_6^+}$ final state that would be formed, in concert with Mu···AuNP in (R2), or to undergo rapid SE[55,56] with the surface electrons, likely leading to complete depolarization of the muon spin and hence no ALC signal at all.

That there are clear ALC signals seen for $\mathrm{Mu\dot{C}_6H_6}$ at this low loading suggests two possible outcomes: (i) either the radical is located at bare silica sites, which would run counter to previous arguments and to the trend seen in Figure 9, or (ii) that the unpaired electron of the radical is *not* in direct contact with the metal surface. We are inclined to the latter view, based as well on the *widths* of the Δ_1 resonances given in Table 1 for all the AuNPs studied herein. If the radical electron were in direct contact with the metal surface, any ALC signal should be *much* broader than on the bare silica, if observed at all, again contrary to observation.

It is also worth pointing out here that the aforementioned ESR detection of spin-trapped $\mathrm{H\dot{C}_6H_6}$ on a Pd catalyst, encapsulated in silica and alumina environments in ref 16, demonstrated that the unpaired electron is *stable* on the radical over the lifetime of the ESR measurement in these oxides. Could this be suggesting that Pd is less metallic in such environments? If so, could that also be the case for the AuNPs encapsulated in SBA-15 silica herein? It is known that finite size effects can alter the density of states for electron energy levels at lower temperatures compared to the band structure seen in bulk metal at higher temperatures.[77,78] Could something similar be at play here? In addition, could the efficacy of a nominally expected transfer of the unpaired electron from the radical to the AuNP surface depend on the geometry of the radical, given its canted orientation on the surface established in P1, thereby affecting its interaction with that surface?

These are complex systems that lead to alternate suggestions for possible reaction mechanisms. Thus, partly in response to the questions raised above as well as to address the likely possibility mentioned earlier that the unpaired electron on the $\mathrm{Mu\dot{C}_6H_6}$ radical is not in contact with the metal surface in this study, an alternate mechanism to (R2) is proposed in (R3), in which the *intermediate* $\mathrm{Mu\dot{C}_6H_6^*}$ state from (R1, R2) on the AuNP surface undergoes an electron transfer from the radical *prior* to forming stabilized $\mathrm{Mu\dot{C}_6H_6}$, as in

$$\mathrm{Mu} + \mathrm{AuNP}/\mathrm{C_6H_6} \rightarrow \underset{\mathrm{H_6{\cdot}AuNP}\uparrow}{\mathrm{Mu\dot{C}_6H_6^*{\cdot}AuNP}} \xrightarrow{[f,\ k_S]} \mathrm{Mu\dot{C}_6H_6} \xrightarrow{[(1-f),\ k_E]} \mathrm{MuC_6H_6^+}\cdots\mathrm{AuNP^-} \quad \text{(R3)}$$

where *f* has the same meaning as in (R2), here in competition with electron transfer from $\mathrm{Mu\dot{C}_6H_6^*}$ to the metal surface, with rate constant k_E. Such a mechanism would imply that electron transfer is facilitated by thermal excitation populating low-lying vibrational states in $\mathrm{Mu\dot{C}_6H_6}$, also addressed in a different context in ref 79, but here giving the diamagnetic final state previewed above. This process might also be influenced by plasmon excitation on these metal NPs, arising via this energy transfer process on the gold NP surfaces,[80] also thought to play a role in macro and mesoporous silica supports for silver NP catalysts.[10]

Coment: Eqns are now correct, including (R3) above. Common to these proposed mechanisms, starting with the basic scheme in (R1), is the formation of a stabilized $\mathrm{Mu\dot{C}_6H_6}$ radical on the AuNP metal surface. This premise only recasts a basic question raised earlier though. Why doesn't this stabilized $\mathrm{Mu\dot{C}_6H_6}$ radical also not lose its unpaired electron to the metal NP surface or give rise to rapid electron SE with the surface electrons, leading to overly broad signals that would likely escape detection? We suggest that this may be due to the geometry of the $\mathrm{Mu\dot{C}_6H_6}$ radical on the surface and how strongly bound it is to that surface, both of which relate to earlier studies of muoniated cyclohexadienyl[7] and of the Mu-*t*-butyl radical[81] in NaY zeolite.

In ref 7, the $\mathrm{Mu\dot{C}_6H_6}$ radical was found to be *strongly* interacting with $\mathrm{Na^+}$ sites in NaY, giving rise to a marked distortion of its normal planar geometry and hence to *two* Δ_1 resonances from inequivalent C−Mu bond orientations, above (exo) and below (endo) the plane, with dramatically different muon hfcc of ±20%, respectively. Given this strong interaction, a Δ_0 resonance due to electron charge density transferred from the radical to the cation was expected,[7,17,82] but, surprisingly, *not* observed,[7] suggesting that this geometric distortion mitigates against electron transfer from $\mathrm{Mu\dot{C}_6H_6}$ to the $\mathrm{Na^+}$. Somewhat counterintuitively though, such a transfer was seen though for the Mu-*t*-butyl radical in NaY,[81] even given its weaker interaction with the Na cations, inferred by the observation of only a single Δ_1 resonance. These contrasting results suggest a subtle interplay between the geometry of the stabilized $\mathrm{MuC_6H_6}$ radical in (R2) and (R3) and the likelihood of electron transfer to the AuNP surface.

We propose then that the canted orientation of the $\mathrm{Mu\dot{C}_6H_6}$ radical on the AuNPs, discussed in P1 and outlined above, may have a similar effect as that seen due to its geometric distortion from planarity in NaY,[7] possibly leading to a shift in electron

https://doi.org/10.1021/acs.jpcc.1c05723
J. Phys. Chem. C 2021, 125, 21410−21423

density in the ring of the muoniated cyclohexadienyl radical, while largely preserving its resonance stability on that surface. Though ion-dipole forces are involved in the case of $Mu\dot{C}_6H_6$ interacting with Na cations in NaY, in contrast to the present study of this neutral radical interacting with a neutral metal NP surface, that is also the case for the Mu-*t*-butyl radical interacting with NaY, where clear Δ_0 resonances were observed, arising from this electron charge transfer.[81] Though the nature of these interactions are bound to differ, given their differences in molecular structure and geometry, there does indeed seem to be grounds for postulating a subtle interplay here between the geometry and localized charge density of the $Mu\dot{C}_6H_6$ radical in its interaction with the AuNP surface, with the surface electrons surely playing a role as well.

The only other ALC study similar to the present one that we know of is the paper of Schwager et al.,[13] in which benzene was added to *nonporous* 7 nm Cabosil silica grains that supported PdNPs of a similar size as the AuNPs studied here, somewhat in parallel then with the ESR study of Carley et al.[16] discussed above. In the μSR study of ref 13, the Mu atom, formed within the silica grains, diffuses into the voids between grains, first explored by Marshall et al.,[83] where it could react with benzene adsorbed on the external surface, as in (R1), with the $Mu\dot{C}_6H_6$ radical formed then expected to diffuse on the surface to a PdNP. The Δ_0 resonances seen in ref 13 showed a clear reduction in amplitude in the Pd-loaded sample compared to bare silica, by about 50%, similar to that seen at comparable benzene loadings on the bare silica and AuNPs in Table 1 here. This was attributed in ref 13 to a "sink" for Mu atoms reacting with the Pd metal prior to reaching the surface-adsorbed Bz, in like manner to chemisorbed Mu on the AuNPs forming diamagnetic muon states on the surface, explored in refs 3 and 5 herein.

In ref 13, it was concluded that the diffusion rate of the $Mu\dot{C}_6H_6$ radical on the Cabosil surface was too slow to reach a PdNP on the μs time scale of the muon lifetime. Were that to happen, given that the BE of Bz to Pd is much stronger than to Au, one would certainly expect to see a shift in resonance positions to lower fields, commented on in ref 13 and above with respect to Figure 7 here. In the present work, we can be quite confident that the Mu atom reacts with surface-adsorbed Bz on the AuNPs, since both the NPs and the benzene are located in the *same* mesopores that the Mu atom diffuses into and out of. An important difference here, as well, is that Bz appears to be only *weakly* adsorbed to the AuNP surface, thereby preserving the resonance stability of the $Mu\dot{C}_6H_6$ radical formed. Beyond noting these differences though, it is difficult to realistically compare the current results in mesoporous silica for different AuNPs and over a range of Bz loadings, wherein the Mu atom diffuses within mesopores encountering Bz/AuNPs therein, with those of ref 13, where the $Mu\dot{C}_6H_6$ radical diffuses on the external surface of the 7 nm Cabosil silica grain. For smaller-sized Cabosil grains, closer to about 3.5 nm, where Mu diffusion into the voids is much more facile,[83] and for the same metal NPs, one could expect the results for porous and nonporous silica to be more directly comparable.

5. CONCLUDING REMARKS

There are several important points arising from this study, that also resonate with our earlier report of reaction rates in paper P1 (ref 5), summarized in Table 1 and plotted in Figure 9, as itemized below:

- The muonium atom (Mu = μ^+e^-), formed in the grains of the SBA-15 silica samples, thermalizes in the silica mesopores, where the encapsulated AuNPs and added benzene (Bz) reactant are also located.
- Mu then reacts primarily with surface-adsorbed Bz on these AuNPs (or with Bz at SiO_2 sites in bare silica) in the silica mesopores, forming the muoniated free radical, $Mu\dot{C}_6H_6$, identified by the μSR technique of avoided level crossing resonance.
- As in P1, it is proposed that the $Mu\dot{C}_6H_6$ radical, formed in reaction schemes (R1)−(R3) from surface-adsorbed Bz on the AuNPs, remains canted on and weakly interacting with the AuNP surface, thus giving rise to ALC resonance positions and hence hfcc that do not change with environment or Bz loading. This is in accord with previously established results of the resonance stability of muoniated cyclohexadienyl in a variety of different environments.
- The $\Delta_1(A_\mu)$ and Δ_0 (A_p) ALC resonances on these AuNPs are seen at LFs of ∼19 and 21 kG, respectively. There is *no evidence* for any additional ALC resonances at lower fields (Figure 7), which would have been the case if the unpaired electron on the $Mu\dot{C}_6H_6$ radical were further delocalized due to a strong binding with the AuNP surface.
- The positions of these ALC resonances do not distinguish the binding sites of $Mu\dot{C}_6H_6$ at either SiO_2 or AuNP sites in these AuNP/silica samples, but their *peak intensities* arguably do provide this distinction, revealing as much as a 10-fold loss in amplitude for $Mu\dot{C}_6H_6$ formed at AuNP sites across the full range of Bz loadings up to 250 Torr in Figure 9, compared to the results for bare silica. This strongly suggests that the benzene in these AuNP/silica samples is primarily located *on/at* the AuNPs and not at the many more plentiful silica sites. See also Figure 8.
- Though preference for $Mu\dot{C}_6H_6$ interacting with AuNP sites is established, the possibility that this radical could also be located at SiO_2 sites in the AuNP/silica samples cannot be ruled out.
- A key question raised herein is why is the $Mu\dot{C}_6H_6$ radical seen at all on these metal AuNP surfaces? Common wisdom would suggest that any radical, *if* in contact with the metal NP surface, would either quickly lose its unpaired electron to that surface or rapid SE of this electron with the conduction electrons on the metal surface would give rise to a fully depolarized muoniated radical.
- This led to our supposition that the canted orientation of the $Mu\dot{C}_6H_6$ radical on these AuNPs leads to a shift in electron charge density, such that the unpaired electron is *not* in direct contact with the metal surface, mandating accurate quantum chemistry calculations to verify. Further studies on different metal NPs, including those that are magnetic, would also be helpful here.

Both this paper and its predecessor (P1) relate to the role played by free radical intermediates in heterogeneous catalysis in silica environments, and in particular here in mesoporous SBA-15 silica. These environments are generally important in such catalysis processes due to their likelihood of facilitating proton or H-atom transfer reactions, forming a true free-radical intermediate state that is expected to play a role in a complex

https://doi.org/10.1021/acs.jpcc.1c05723
J. Phys. Chem. C 2021, 125, 21410−21423

catalytic sequence of fundamental reaction steps in these environments. It is this context that provided motivation for the present study of the isotopic hydrogenic Mu atom in studying the specific reaction step forming Mu-adduct cyclohexadienyl radicals analogous to $\dot{HC}_6H_6$ in mesoporous (SBA-15) silica. Though ESR would generally be the technique of choice for such H-atom studies, its efficacy can be highly compromised due to radical−radical recombination reactions in the constricted spaces of the silica mesopores.

AUTHOR INFORMATION

Corresponding Author

Donald G. Fleming − *TRIUMF and Department of Chemistry, University of British Columbia, Vancouver, BC, Canada V6T1Z1*; orcid.org/0000-0002-6552-7044; Email: flem@triumf.ca

Authors

William A. MacFarlane − *TRIUMF and Department of Chemistry, University of British Columbia, Vancouver, BC, Canada V6T1Z1*

Jiyu Xiao − *TRIUMF and Department of Chemistry, University of British Columbia, Vancouver, BC, Canada V6T1Z1*

Donald J. Arseneau − *CMMS Facility, TRIUMF, Vancouver, BC, Canada V6T2A3*

Robert F. Kiefl − *TRIUMF and Department of Physics & Astronomy, University of British Columbia, Vancouver, BC, Canada V6T1Z1*

Yuanyuan Cao − *School of Materials Science and Engineering, East China University of Science & Technology, Shanghai 200237, China*

Peixi-X Wang − *Suzhou Institute of Nano-Tech and Nano-Bionics, Chinese Academy of Sciences, Suzhou, Jiangsu 215123, P. R. China*; orcid.org/0000-0003-0683-4818

Mark J. MacLachlan − *Department of Chemistry, University of British Columbia, Vancouver, BC V6T1Z1, Canada*; orcid.org/0000-0002-3546-7132

Michael D. Bridges − *Jules Stein Eye Institute, University of California, Los Angeles, California 90095, United States*

Complete contact information is available at: https://pubs.acs.org/10.1021/acs.jpcc.1c05723

Notes

The authors declare no competing financial interest.

ACKNOWLEDGMENTS

D.G.F., W.A.M., R.F.K., and M.J.M. gratefully acknowledge the financial support of the Natural Sciences and Engineering Research Council of Canada (NSERC). The help of Mr. Martin Dehn in the data taking was also greatly appreciated.

REFERENCES

(1) Daniel, M. C.; Astruc, D. Gold Nanoparticles: Assembly, Supramolecular Chemistry, Quantum-Size-Related Properties, and Applications toward Biology, Catalysis, and Nanotechnology. *Chem. Rev.* **2004**, *104*, 293−346.

(2) Nealon, G. J.; Donnio, B.; Greget, R.; Kappler, J.-P.; Terazzi, E.; Gallani, J.-L. Magnetism in gold nanoparticles. *Nanoscale* **2012**, *4*, 5244−5258.

(3) Dehn, D. H.; Arseneau, D. J.; Böni, P.; Bridges, M. D.; Buck, T.; Cortie, D. L.; Fleming, D. G.; Kelly, J. A.; MacFarlane, W. A.; MacLachlan, M. J.; et al. Communication: Chemisorption of muonium on gold nanoparticles: A sensitive new probe of surface magnetism and reactivity. *Communication. J. Chem. Phys.* **2016**, *145*, 181102−5.

(4) Dehn, M. H.; Arseneau, D. J.; Buck, T.; Cortie, D. L.; Fleming, D. G.; MacFarlane, W. A.; King, S. R.; McDonagh, A. M.; McFadden, R. M. L.; Mitchell, D. R. G.; Kiefl, R. F. Nature of magnetism in thiol-capped gold nanoparticles investigated with Muon spin rotation. *Appl. Phys. Lett.* **2018**, *112*, 053105.

(5) Fleming, D. G.; MacFarlane, W. A.; Xiao, J.; Arseneau, D. J.; Dehn, M. H.; Kiefl, R. F.; Zamarion, V. M.; Wang, P. X.; Cao, Y.; MacLachlan, M. J.; Bridges, M. D. Studies of Muonium Reactivity with Uncapped Gold Nanoparticles and with Surface-Adsorbed Benzene on These NPs in Porous Silica Hosts. *J. Phys. Chem. C* **2019**, *123*, 27628−27642.

(6) Yang, X.-F.; Wang, A.-Q.; Wang, W.-L.; Zhang, T.; Li, J. Unusual Selectivity of Gold Catalysts for Hydrogenation of 1,3-Butadiene toward cis-2-Butene: A Joint Experimental and Theoretical Investigation. *J. Phys. Chem. C* **2010**, *114*, 3131−3139.

(7) Fleming, D. G.; Arseneau, D. J.; Shelley, M. Y.; Beck, B.; Dilger, H.; Roduner, E. μSR Studies of Hyperfine Couplings and Molecular Interactions of the Mu-Cyclohexadienyl Radical in Y-Zeolites and in Solid Bulk Benzene. *J. Phys. Chem. C* **2011**, *115*, 11177−11196.

(8) Alba-Molina, M.; Puente Santiago, A. R.; Giner-Casares, J. J.; Martín-Romero, M. T.; Camacho, L.; Luque, R.; Cano, M. Citrate-Stabilized Gold Nanoparticles as High-Performance Electrocatalysts: The Role of Size in the Electroreduction of Oxygen. *J. Phys. Chem. C* **2019**, *123*, 9807−9812.

(9) Dong, B.; Mansour, N.; Pei, Y.; Wang; Huang, T.; Filbrun, S. L.; Chen, M.; Cheng, X.; Pruski, M.; Huang, W.; Fang, N. Single Molecule Investigation of Nanoconfinement Hydrophobicity in Heterogeneous Catalysis. *J. Am. Chem. Soc.* **2020**, *142*, 13305−13309.

(10) Yamazaki, Y.; Kuwahara, K.; Mori, K.; Kamegawa, t.; Yamashita, H. Enhanced Catalysis of Plasmonic Silber Nanoparticles by a Combination of Macro-/Mesoporous Nanostructured Silica Support. *J. Phys. Chem. C* **2021**, *125*, 9150−9157.

(11) Xiao, J.; Arseneau, D. J.; Bridges, M. D.; Cortie, D.; Cottrell, S. P.; Dehn, M.; Fleming, D. G.; Kelly, J.; Kiefl, R. F.; MacFarlane, W. A.; et al. Interaction of the Mu-cyclohexadienyl radical with metallic (Au, Pt) nanoparticles in mesoporous silica. *Journal of Physics: Conf. Series* **2014**, *551*, 012044−1.

(12) Kidder, M. K.; Buchanan, A. C., III Effect of Pore Confinement and Molecular Orientation on Hydrogen Transfer During a Free-Radical Reaction in Mesoporous Silica. *J. Phys. Chem. C* **2008**, *112*, 3027−3031.

(13) Schwager, M.; Dilger, H.; Roduner, E.; Reid, I. D.; Percival, P. W.; Baiker, A. Surface difusion of the cyclohexadienyl radical adsdorbed on silica and on a silica-suppported Pd catalyst studied by means of ALC-μSR. *Chem. Phys.* **1994**, *189*, 697−712.

(14) Yun, J. H.; Lobo, R. F. Radical Cation Intermediates in Propane Dehydrogenation and Propene Hydrogenation over H-[Fe] Zeolites. *J. Phys. Chem. C* **2014**, *118*, 27292−27300.

(15) Werst, D. W.; Han, P.; Choure, S. C.; Vinokur, E. I.; Xu, L.; Trifunac, A. D.; Eriksson, L. A. Hydrogen Atom Addition to Hydrocarbon Guests in Radiolyzed Zeolites. *J. Phys. Chem. B* **1999**, *103*, 9219.

(16) Carley, A. F.; Edwards, H. A.; Mile, B.; Roberts, M. W.; Rowlands, C. G.; Hancock, F. E.; Jackson, D. S. Applications of EPR to a study of the hydrogenation of ethene and benzene over a supported Pd catalyst: detection of free radicals on a catalyst surface. *J. Chem. Soc., Faraday Trans.* **1994**, *90*, 3341.

(17) Fleming, D. G.; Shelley, M. Y.; Arseneau, D. J.; Senba, M.; Pan, J. J.; Roduner, E. Hyperfine and Host-Guest Interactions of the Mu-cyclohexadienyl Radical in NaY Zeolite. *J. Phys. Chem. B* **2002**, *106*, 6395−6407.

(18) Zhang, Z.; Berg, A.; Levanon, H.; Fessenden, R. W.; Meisel, D. On the Interaction of Free Radicals with Gold Nanoparticles. *J. Am. Chem. Soc.* **2003**, *125*, 7959−7963.

(19) Cuadrado, R.; Puerta, J. M.; Soria, F.; Cerda, J. I. A first principles study of thiol-capped Au nanoparticles: Structural,

electronic, and magnetic properties as a function of thiol coverage. *J. Chem. Phys.* **2013**, *139*, 034319.
(20) Pensa, E.; Albrecht, T. Controlling the Dynamic Instability of Capped Metal Nanoparticles on Metallic Surfaces. *J. Phys. Chem. Lett.* **2018**, *9*, 57−62.
(21) Fleming, D. G.; Manz, J.; Sato, K.; Takayanagi, T. Fundamental Change in the Nature of Chemical Bonding by Isotopic Substitution. *Angew. Chem., Int. Ed.* **2014**, *53*, 13706−13709.
(22) Roduner, E. Polarized positive muons probing free radicals: a variant of magnetic resonance. *Chem. Soc. Rev.* **1993**, *22*, 337−346.
(23) Dehn, M. H.; Cao, Y.; Wang, P.-X.; Cottrell, S. P.; MacLachlan, M. J.; Fleming, D. G.; Kiefl, R. F. Direct observation of muonium reacting with uncapped gold nanoparticles in porous silica and nature of the final state. *J. Chem. Phys.* **2020**, *152*, 184706.
(24) Song, H.; Rioux, R. M.; Hoefelmeyer, J. D.; Komor, R.; Niesz, K.; Grass, M.; Yang, P.; Somorjai, G. A. Hydrothermal Growth of Mesoporous SBA-15 Silica in the Presence of PVP-Stabilized Pt Nanoparticles: Synthesis, Characterization and Catalytic Properties. *J. Am. Chem. Soc.* **2006**, *128*, 3027−3037.
(25) Dehn, M. H.; Fleming, D. G.; MacFarlane, W. A.; MacLachlan, M. J.; Zamarion, V. M.; Kiefl, R. F. Dynamics of anisotropic muonium on silica surfaces explained by Monte Carlo simulation of the muon depolarization. *JPS Conf. Proc.* **2017**, *21*, 011032.
(26) Huang, W.; Li, W.-X. Surface and interface design for heterogeneous catalysis. *Phys. Chem. Chem. Phys.* **2019**, *21*, 523−526.
(27) Metiu, H. Preface to Special Topic: A Survey of Some New Developments in Heterogeneous Catalysis. *J. Chem. Phys.* **2008**, *128*, 182501.
(28) Engel, J.; Francis, S.; Roldan, A. The influence of support materials on the structural and electronic properties of gold nanoparticles- a DFT study. *Phys. Chem. Chem. Phys.* **2019**, *21*, 19011−19025.
(29) Murakami, K.; Sekine, Y. Recent progress in use and observation of hydrogen migration over metal oxides. *Phys. Chem. Chem. Phys.* **2020**, *22*, 22852−22863.
(30) Alothman, Z. A. A Review: Fundamental Aspects of Silicate Mesoporous Materials. *Materials* **2012**, *5*, 2874−2902.
(31) Zhao, E. W.; Maligal-Ganesh, R.; Mentink-Vigier, F.; Zhao, T. Y.; Du, Y.; Pei, Y.; Huang, W.; Bowers, C. R. Atomic-Scale Structure of Mesoporous Silca-Encapsulated Pt and PtSn Nanoparticles Revealed by Dynamic Nuclear Polarization-Enhanced ^{29}Si MAS NMR Spectroscopy. *J. Phys. Chem. C* **2019**, *123*, 7299−7307.
(32) Haw, J. F. Zeolite acid strength and reaction mechanisms in catalysis. *Phys. Chem. Chem. Phys.* **2002**, *4*, 5431.
(33) Yin, J.; Guo, X.; Sun, Y.; Han, S.; Li, Q. Understanding the Nanoconfinement Effect on the the Ethanol-to-Propene Mechanism Catalyzedd by Acidic ZSM = 5 and FAU Zeolites. *J. Phys. Chem. C* **2021**, *125*, 310−334.
(34) Mezari, B.; Magusin, P. C. M. M.; Almutairi, S. M. T.; Pidko, E. A.; Hensen, E. J. M. Nature of Enhanced Bronsted Acidity Induced by Extraframework Aluminum in an Ultrastabilized Faujasite Zeolite: An *in Situ* NMR Study. *J. Phys. Chem. C* **2021**, *125*, 9050−9059.
(35) Hensen, E. M. J.; Poduval, D. G.; Ligthart, D. A. J. M.; van Veen, J. A. R.; Rigutto, M. S. Quantification of Brøsted Acid Sites in Aluminosilicates. *J. Phys. Chem. C* **2010**, *114*, 8363−8374.
(36) Gierada, M.; De Proft, F.; Sulpizi, M.; Tielens, F. Understanding the Acidic Properties of the Amorphous Hydroxlated Silica Surface. *J. Phys. Chem. C* **2019**, *123*, 17343−17352.
(37) Vu, K. B.; Bach, L. G.; Van Tran, T.; Thuong, N. T.; Giang, H. N.; Bui, Q. T. P.; Ngo, S. T. Gold@silica catalyst: Porosity of silica shells switches catalytic reactions. *Chem. Phys. Lett.* **2019**, *728*, 80−86.
(38) Zalazar, F. M.; Cabral, N. D.; Romero Ojeda, G. D.; Alégre, C. I. A.; Peruchena, N. M. Confinement Effects in Protonation Reactions Catalyzed by Zeolites with Large Void Structures. *J. Phys. Chem. C* **2018**, *122*, 27350−27359.
(39) Venuto, P. B. in Catalysis by Zeolites: International Symposium Proceedings. *Stud. Surf. Sci. Catal.* **1997**, *105*, 811.
(40) Lutterloh, C.; Biener, J.; Schenk, A.; Küppers, J. Interaction of D(H) atoms with physisorbed benzene and (1,4)- dimethylcyclohexane: Hydrogenation and H abstraction. *J. Chem. Phys.* **1996**, *104*, 2392−2400.
(41) Rhodes, C. J.; Butcher, E. C.; Morris, H.; Reid, I. D. Mobility of Radicals in Zeolite Catalysts: Molecular Motion Studied by Muon Spectroscopy. *Magn. Reson. Chem.* **1995**, *33*, S134−S146.
(42) Roduner, E.; Schwager, M.; Tregenna-Piggott, P.; Dilger, H.; Shelley, M.; Reid, I. D. Dynamics of the Cyclohexadienyl Radical Adsorebed in Porous Silica and NaZSM5. *Ber. Bunsenges. Phys. Chem.* **1995**, *99*, 1338−1342.
(43) Bridges, M. D.; Arseneau, D. J.; Fleming, D. G.; Ghandi, K. Hyperfine Interactions and Molecular Motion of the Mu-Ethyl Radical in Faujasites: NaY, HY, USY. *J. Phys. Chem. C* **2007**, *111*, 9779−9793.
(44) Roduner, E.; Dilger, H. Acid Catalysis in HSM-5: The Role of Entropy. *J. Am. Chem. Soc.* **2001**, *123*, 7717.
(45) Fleming, D. G.; Arseneau, D. J.; Pan, J. J.; Shelley, M. Y.; Senba, M.; Percival, P. W. Hyperfine Coupling Constants of Muonium-substituted cyclohexadienyl radicals (C6H6Mu, C6D6Mu and C6F6Mu) in the Gas Phase. *Appl. Magn. Reson.* **1997**, *13*, 181.
(46) Yu, D.; Percival, P. W.; Brodovitch, J.-C.; Leung, S. K.; Kiefl, R. F.; Venkateswaran, K.; Cox, S. F. J. Structure and Intramolecular Motion of Muonium-Substituted Cyclohexadienyl Radicals. *Chem. Phys.* **1990**, *142*, 229.
(47) Dervin, D.; O'Malley, A. J.; Falkowska, M.; Chansai, S.; Silverwood, I. P.; Hardacre, C.; Catlow, C. R. A. Probing the dynamics and structure of confined benzene in MCM-41 based catalysts. *Phys. Chem. Chem. Phys.* **2020**, *22*, 11485−11489.
(48) Kaprinidis, N. A.; Landis, M. S.; Turro, N. J. Supramolecular control of photochemical enantiomeric induction and radical pair recombination in zeolites. *Tetrahedron Lett.* **1997**, *38*, 2609.
(49) Rubinovich, E.; Polak, M. Unraveling the Distinct Relationship between the Extent of a Nanoconfined Reaction and the Equilibrium Constant. *J. Phys. Chem. C* **2021**, *125*, 452−457.
(50) Roduner, E. Muon Spin Resonance-A variant of magnetic resonance. *Appl. Magn. Reson.* **1997**, *13*, 1.
(51) Roduner, E. Muons in Physics, Chemistry and Materials. In *Proceedings of St. Andrews Summer School in Physics*; NATO Advanced Study Institute, August 1998; Lee, S. L., Kilcoyne, S. H., Cywinski, R., Eds.; Scottish Universities Summer School in Physics & Institute of Physics Publishing: Bristol and Philadelphia, 1998.
(52) Kiefl, R. F.; Kreitzman, S.; Celio, M.; Keitel, R.; Luke, G. M.; Brewer, J. H.; Noakes, D. R.; Percival, P. W.; Matsuzaki, T.; Nishiyama, K. Resolved nuclear hyperfine structure of a muonated free radical using level-crossing spectroscopy. *Phys. Rev. A: At., Mol., Opt. Phys.* **1986**, *34*, No. 681.
(53) Kiefl, R. F. Level-crossing Resonance in Muonium-like Systems. *Hyperfine Interact.* **1986**, *32*, 707−720.
(54) Heming, M.; Roduner, E.; Patterson, B. D.; Odermatt, W.; et al. Detection of muonated free radicals through the effects of avoided level crossing. Theory and analysis of spectra. *Chem. Phys. Lett.* **1986**, *128*, 100.
(55) Kreitzman, S. R. Electron relaxation dynamics of Mu ALCR spectra. *Chem. Phys.* **1991**, *152*, 353−364.
(56) Kreitzman, S. R.; Roduner, E. Theory of avoided level-crossing relaxation dynamics for axal muonated radicals. *Chem. Phys.* **1995**, *192*, 189−230.
(57) Roduner, E.; Stolmár, M.; Dilger, H.; Reid, I. D. Reorientational Dynamics of Cyclohexadienyl Radicals in High-Silica ZSM-5. *J. Phys. Chem. A* **1998**, *102*, 7591−7597.
(58) Roduner, E. Radical Reorientation Dynamics Studied by Positive-Muon Avoided Level Crossing Resonance. *Hyperfine Interact.* **1991**, *65*, 857.
(59) Senba, M.; Arseneau, D. J.; Pan, J. J.; Fleming, D. G. Slowing-down times and stopping powers for ∼ 2- MeV μ^+ in low-pressure gases. *Phys. Rev. A: At., Mol., Opt. Phys.* **2006**, *74*, 042708−17.
(60) Johnson, C.; Cottrell, S. P.; Ghandi, K.; Fleming, D. G. Muon implantation in inert gases studied by radio frequency spectroscopy. *J. Phys. B: At., Mol. Opt. Phys.* **2005**, *38*, 119−134.

https://doi.org/10.1021/acs.jpcc.1c05723
J. Phys. Chem. C 2021, 125, 21410−21423

(61) Aslyamov, T.; Khlyupin, A.; Pletneva, V.; Akhatov, I. Theoretical Approach to Rough Surface Characterization for Silica Materials. *J. Phys. Chem. C* **2019**, *123*, 28707−28714.
(62) Alan, B. O.; Barisik, M.; Ozcelik, H. G. Roughness Effects on the Surface Charge Properties of Silica Nanoparticles. *J. Phys. Chem. C* **2020**, *124*, 7274−7286.
(63) Martyniak, A.; Dilger, H.; Scheuermann, R.; Tucker, I. M.; McKenzie, I.; Vujosevic, D.; Roduner, E. Using spin polarized positive muons for studying guest molecule partioning in soft matter structures. *Phys. Chem. Chem. Phys.* **2006**, *8*, 4723.
(64) Falkowska, M.; Bowron, D. T.; Manyar, H.; Youngs, T. G. A.; Hardacre, C. Confinement Effects on the Benzene Orientational Structure. *Angew. Chem., Int. Ed.* **2018**, *57*, 4565.
(65) Bhattacharjee, S.; Lee, S.-C. Cooperation and competition between magnetism and chemisorption. *Phys. Chem. Chem. Phys.* **2021**, *23*, 3802−3809.
(66) Hochstrasser, J.; Svidrytski, A.; Höltzel, A.; Priamushko, R.; Kleitz, F.; Wang, W.; Kübel, C.; Tallarek, U. Morphology-transport relationships for SBA-15 and KIT-6 ordered mesoporous silicas. *Phys. Chem. Chem. Phys.* **2020**, *22*, 11314−11326.
(67) Chakraborty, D.; Chattaraj, P. K. Bonding, Reactivity, and Dynamics in Confined Systems. *J. Phys. Chem. A* **2019**, *123*, 4513−4531.
(68) Xue, M.; Zink, J. I. Probing the Microenvironment in the Confined Pores of Mesoporous Silica Nanoparticles. *J. Phys. Chem. Lett.* **2014**, *5*, 839−842.
(69) Alba-Simionesco, E.; Coasne, B.; Dosseh, G.; Dudziak, G.; Gubbins, K. E.; Radhakrishnan, R.; Sliwinska-Bartkowiak, M. Effects of confinement on freezing and melting. *J. Phys.: Condens. Matter* **2006**, *18*, R15−R68.
(70) Roduner, E. *Nanoscopic Materials: Size-Dependent Phenomena and Growth Principles*, 2nd ed., Royal Society of Chemistry: 2014.
(71) Carter-Fenk, K.; Herbert, J. M. Reinterpreting π-stacking. *Phys. Chem. Chem. Phys.* **2020**, *22*, 24870−24886.
(72) Lee, J.; Dougherty, D. B.; Yates, J. T. Edoge-on Bonding of Benzene Molecules in the Second Adsorbed Layer on Cu(110). *J. Phys. Chem. B* **2006**, *110*, 15645−15649.
(73) Chiang, Y.-D.; Lian, H.-Y.; Leo, S.-Y.; Wang, S.-G.; Yamauchi, Y.; Wu, K. C.-W. Controlling Particle Size and Structural Properties of Mesoporous Silica Nanoparticles Using the Taguchi Method. *J. Phys. Chem. C* **2011**, *115*, 13158−13165.
(74) Li, J.; Zhang, Y.; Zheng, J. Intermolecular energy flows between surface molecules on metal nanoparticles. *Phys. Chem. Chem. Phys.* **2019**, *21*, 4240−4245.
(75) Liu, W.; Maass, F.; Willenbockel, M.; Bronner, C.; Schulze, M.; Soubatch, S.; Tautz, F. S.; Tegeder, P.; Tkatchenko, A. Quantitative Prediction of Molecular Adsorption: Structure and Binding of Benzene on Coinage Metals. *Phys. Rev. Lett.* **2015**, *115*, 036104.
(76) Laoufi, I.; Saint-Lager, M. C.; Lazzari, R.; Jupille, J.; Robach, O.; Garaudée, D. S.; Cabailh, G.; Dolle, P.; Cruguel, H.; Bailly, A. Size and Catalytic Activity of Supported Gold Nanpoarticles:An in Operando Study during CO Oxidation. *J. Phys. Chem. C* **2011**, *115*, 4673−4679.
(77) Nilius, N.; Wallis, T. M.; Ho, W. Development of One-Dimensional Band Structure in Artificial Gold Chains. *Science* **2002**, *297*, 1853−1856.
(78) van der Klink, J. J.; Brom, H. NMR in metals, metal particles and metal clusters. *Prog. Nucl. Magn. Reson. Spectrosc.* **2000**, *36*, 89−201.
(79) Abraham, B.; Rego, L. G. C.; Gundlach, L. Electronic-Vibrational Coupling and Electron Transfer. *J. Phys. Chem. C* **2019**, *123*, 23760−23772.
(80) Ding, W.; Hsu, L.-Y.; Schatz, G. C. Plasmon-coupled resonance energy transfer: A real-time electrodynamics approach. *J. Chem. Phys.* **2017**, *146*, 064109.
(81) Fleming, D. G.; Arseneau, D. J.; Bridges, M. D.; Chen, Y. K.; Wang, Y. A. Hyperfine Coupling Constants of the Mu-t-Butyl Radical in NaY and USY Compared with Similar Data in the Bulk and with Ab Initio Theory. *J. Phys. Chem. C* **2013**, *117*, 16523−16539.
(82) Webster, B.; Macrae, R. M. A theoretical investigation of the effect of a sodium cation on the proton-electron hyperfine coupling constants of the cyclohexadienyl radical and some consequences for the muonium-substituted cyclohexadienyl radical, C_6H_6, formed in zeolites. *Phys. B* **2000**, *289−290*, 598−602.
(83) Marshall, G. M.; Warren, J. B.; Garner, D. M.; Clark, G. S.; Brewer, J. H.; Fleming, D. G. Production of Thermal Muonium in the Vacuum Between the Grains of Fine Silica Powders. *Phys. Lett. A* **1978**, *65*, 351−358.

https://doi.org/10.1021/acs.jpcc.1c05723
J. Phys. Chem. C 2021, 125, 21410−21423